# A Case Study of Solar Warming and Subsequent Mixing in the Arctic Upper Ocean for the 2011 Spring-Summer Transition

Ara Lee

Undergraduate Senior Thesis

December 2019

Thesis Advisor: Jennifer K. Hutchings

**Abstract**

Autonomous buoys were deployed in 2011 in the central Arctic: An Ice-Tethered Profiler (ITP) and Ice Mass Balance (IMB) buoys were deployed in the Makarov basin; a Polar Ocean Profiling System (POPS) and Ice Thickness (Ice-T) buoy were deployed on the Eurasian Basin. The two different sites were approximately 70km apart. We compare the two different drifting stations to investigate spatial variability associated with heat fluxes near the ice base and spatial water property variability within the surface mixed layer. Our case study follows Vivier et al. (2016) who found the early basal melt onset at the Eurasian Basin site. Focusing on the basal melt onset, we ask the following questions: (1) Do spatial variations in the upper ocean drive the different timing of the basal melt onset? (2) How is the basal melt onset timing affected by these spatial variations? We found spatial differences in upper water properties and melt onset during spring-summer transition. The freshening of surface water at the Eurasian Basin site happens about 20 days earlier than the Makarov Basin site. We identified low ice speed is associated with warming and freshening near the surface, suggesting accumulation of absorbed solar radiation heat near the ice is mixed deeper after quiescent periods. Subsequent mixing affects the vertical heat flux between the water above and below. During surface layer freshening, variability in lead opening and ice motion controls the spatial variability in the mixed layer as well as the basal melt associated with heat flux from the upper ocean to the bottom of the sea ice. At non-quiescent times, in spring, heat flux is related to deeper stratification.

*keywords*: sea ice, basal melt onset, sea ice velocity, heat flux, heat content

## 1. Introduction

The Arctic Ocean plays a role in global climate change due to the sea ice-albedo feedback mechanism, which is controlled by energy exchange processes between the ice, the atmospheric boundary layer and the oceanic boundary layer (Curry et al., 1995; Shaw et al., 2009). Sea ice dominates the exchange processes between the atmosphere and the ocean and therefore alters seasonal and interannual variations at the ocean-atmosphere interface. There have been major changes in the Arctic Ocean, with sea ice experiencing an overall declining trend in its extent, thickness, and age during the last decades (Stroeve et al., 2007; Comiso et al., 2008). Numerical models, designed to simulate the observed sea ice decline and to predict the future conditions of the Arctic, have limitations in resolved physical processes and are conservative in

their predictions of ice extent decline. This is partly due to the lack of observations and physical understanding of the small-scale processes that occur below the sea ice, which contribute to basal melt.

*Sea Ice-Albedo Feedback*

Changes in albedo are critical to the Arctic surface energy budget and regulates heat budgets in the atmosphere, sea ice cover, and upper ocean (Curry et al. 1995). In the Arctic, the largest absorber of solar radiation is the ocean. Due to climate change, decreased sea ice extent causes the ocean to continue to become more exposed to solar radiation. This radiation is absorbed by the ocean, producing a further increase in ocean and atmospheric temperatures. Increased ocean and atmospheric temperatures cause additional ice melt. Solar radiation that enters the under-ice ocean boundary layer (IOBL) when it is either absorbed by open water or transmitted through deep melt ponds and ice, where it is stored as heat (Shaw et al., 2009). When the regional albedo is low, more heat from solar input will be stored in the IOBL. Shaw et al., (2009) and Stanton et al. (2012) determined that the additional heat can become available through ice-generated turbulence to enhance the basal melt, in addition to the surface melt from solar radiation and that heat stored from solar radiation in the IOBL can be transferred from the ocean to the base of the ice and become available for the basal melt of ice.

*Ocean-to-Ice Heat Flux*

The transfer of ocean heat to the ice, the ocean-to-ice heat flux, can be enhanced from increased absorption and transmission of solar radiation in the IOBL (Stanton et al., 2012). The ocean-ice-heat flux is determined by the heat content and turbulence in the IOBL, and the stratification of the pycnocline below the IOBL (Shaw et al. 2009). The heat stored in relatively warm layers below the IOBL cannot be vertical mixing to the ice under normal conditions because of the presence of a strong permanent halocline that acts to dynamically isolate the two layers (Shaw et al. 2009). They also concluded that thin first-year-ice reacts more easily to wind forces, increasing ice-generated turbulence needed to mix heat vertically and make it available for the basal melt of ice.

In this thesis, by particularly focusing on the basal melt onset rather than the top surface melt, we address the following questions: (1) Do spatial variations in the upper ocean drive the

different timing of the basal melt onset? (2) How is the basal melt onset timing affected by these spatial variations?

Bathymetry controls spatial water property variabilities, which is correlated with spatial variations in the regional water masses. Since melt onset is influenced by ocean currents, sea ice motion, and mixing effects (Markus et al., 2009), the different timing of basal melt onset is associated with heat fluxes near the ice base related to the regional mixed layer temperature and salinity changes corresponding to localized warming, near-internal waves and localized eddies. We focus on the period of the transition from late spring to early summer because its timing is identified as the main driver of the Arctic annual energy and mass budgets (Arndt & Nicolaus, 2014). The most pronounced changes occur during the spring-summer transition as sea ice properties in the Arctic are characterized by a distinct seasonal cycle (Perovich et al., 2007; Perovich & Polashenski, 2012). Due to increasing radiative heating and light absorption, liquid water forms within the snow in the upper snowpack. The subsequent melt leads to complete snowmelt and widespread formation of melt ponds at the sea ice surface (Markus et al., 2009).

Arctic sea ice is affected from both surface melting due to atmospheric conditions, as well as basal melting due to oceanic conditions (Shaw et al., 2009; Perovich & Polashenski, 2012). The interannual and regional variability in Arctic sea ice melt has been studied largely in terms of surface melting. The impact of the spatial variability of basal melt onset by physical process of the upper ocean on the mass and energy budgets of sea ice is less studied. Arndt & Nicolaus (2014) recorded an annual increase in light transmission of 1.5 %, with regional maxima up to 4 % over the time period 1979 to 2011. The higher light transmission increases the ocean heat flux, leading to an estimated annual basal ice melt of up to 1.3 m (Arndt & Nicolaus, 2014). These results emphasize the increasing importance of basal melt for the Arctic sea ice mass and energy budget, but there are only few observations documenting small scale (sub-synoptic) variability in basal melt. As the variety of processes related to sea ice emphasizes its importance in the Earth's climate system, it is important to observe small scale variability in basal melt in order to improve our understanding of the role of basal melt variability for sea ice.

The purpose of this study is to compare two different cases which were approximately 70km apart and to investigate spatial variability associated with heat fluxes near the ice base and spatial water property variability within the surface mixed layer. Two different datasets collected

in different basins separated and distinguished by the Lomonosov Ridge in 2011 are used in the comparison. This study will broaden our understanding of the basal melt onset. The physical properties of sea ice and upper water do not only vary in time but also in space. Understanding its spatial variability is important to determine and estimate energy fluxes across the atmosphere, sea ice and ocean boundaries. Therefore, localized sea ice and ocean dynamics will need to be taken into consideration for future basal melt onset studies.

## 2. Data and Methods

We used data collected by autonomous buoys deployed in 2011 to study the upper ocean below sea ice. Ice-Tethered Profilers (ITP) were deployed with companion Ice Mass Balance (IMB) buoys. The data from ITP #47 and IMB 2011C are compared with those from a Polar Ocean Profiling System (POPS) and Ice Thickness (Ice-T) Buoy, comparing the different ocean state between two locations approximately 70km apart. We considered ITP and IMB buoys tracks as Site1 and POPS and Ice-T buoys as Site2. The two tracks are over significantly different bathymetry (Figure 1 and 2). Figure 1 shows ITP #47 and IMB 2011C buoy drift tracks. The Site 1 buoys drifted from Makarov basin to Eurasian basin crossing the Lomonosov Ridge around day of year 175 (Figure 1 and 2). Ice-T\POPS buoys drift tracks, Site 2, stayed in the Eurasian Basin with a drift path that parallels that of Site 1 (Figure 1).

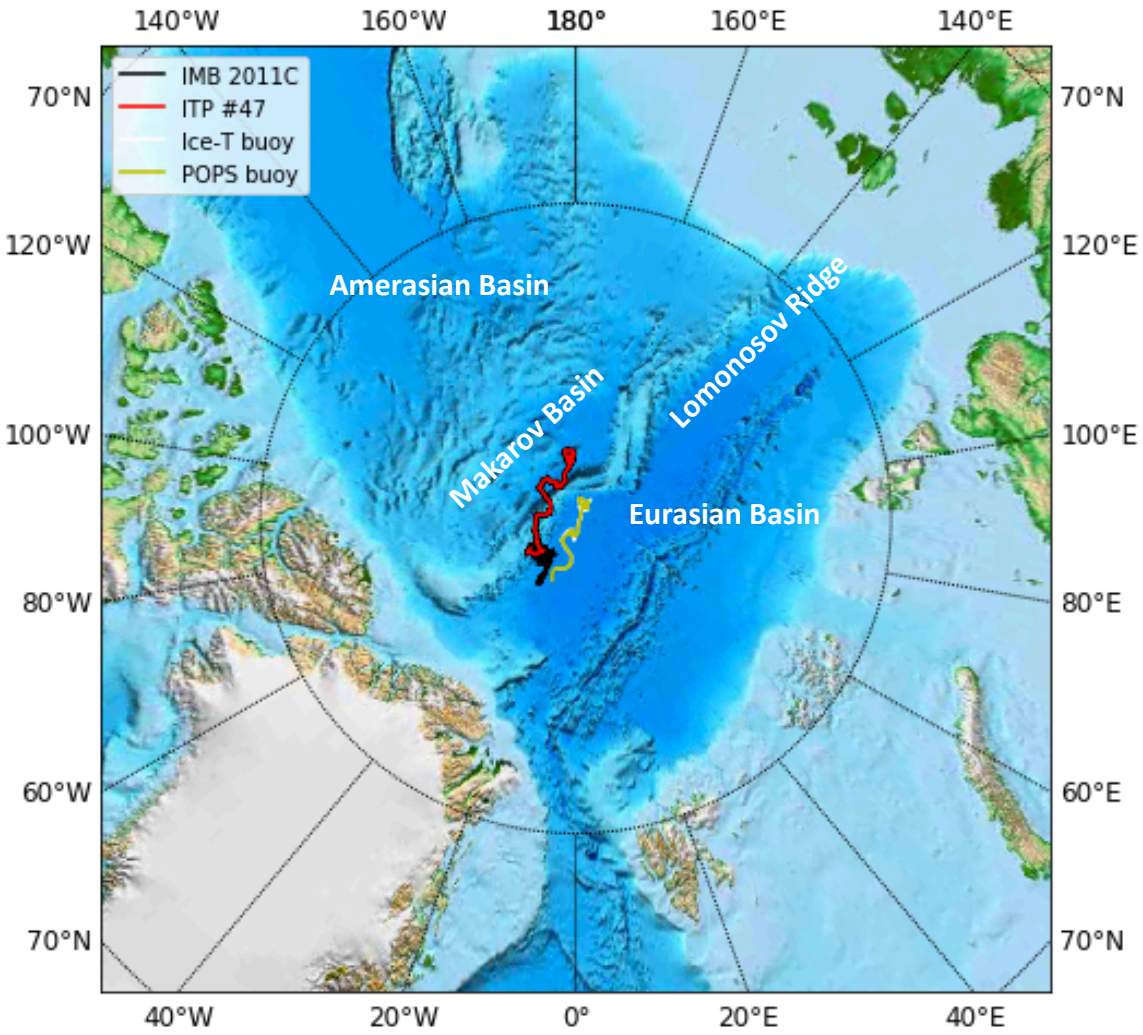


Figure 1. Map showing location of ITP #47 (red), IMB 2011C (black), Ice-T (white) and POPS (yellow) drift trajectories **during days 100-230** in 2011; **Case 1** indicates ITP #47 (red) & IMB 2011C (black); **Case 2** indicates Ice-T (white) & POPS (yellow).

*Bathymetry*

We recognized that the different water mass properties are related to the bathymetry. The water masses differ in the two cases, showing spatial variabilities in temperature, salinity and density. In Figure 2, the Site 2 buoys drifted across relatively smooth and flat bathymetry with depths around 4360 - 3910 m in the Eurasian basin. Compared to Site 1, Site 2 experienced less depth variation. The Lomonosov Ridge is a major topographical feature in the Arctic Ocean (Aagaard et al. 1985; Woodgate et al., 2011; Björk et al., 2018). On the Makarov Basin side of the Lomonosov Ridge, the deep water is distinguished from the Eurasian Basin deep water, which is warmer and more saline than the Makarov Basin (Schauer et al., 2002). Between days 180 and 200, Site 1 buoys were drifting at a relatively shallower depth of 1900-1100 m on the Lomonosov Ridge, while Site 2 buoys were drifting at depth of 4200-4180 m (Figure 2).

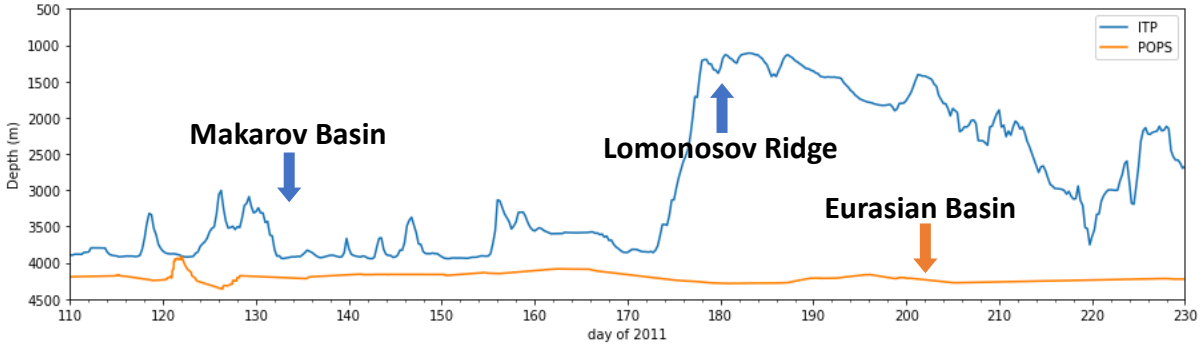


Figure 2. Bathymetry of the ITP #47 and POPS trajectory. Bathymetry is from ETOPO-1.

## 2.1 Site 1

The ITP 47 was deployed on a 3.5 m thick ice-floe in the Transpolar Drift Stream on April 11, 2011, at 87° 59.3'N, 178°30.5'W. The ITP instrument is composed of three main components: a surface instrument package that typically sits atop an ice floe, a weighted, wire-rope tether goes to the ice. An instrumented underwater profiler travels up and down the wire tether to 7m below the ice (Krishfield et al., 2008). The profiling unit measures temperature, salinity and pressure. ITP 47 gathered temperature and salinity data at about 25 cm vertical resolution on four profiles each day from 7 m to 760 m depth with an accuracy of 0.005 or less PSU and 0.001-0.002 °C, respectively (Toole et al., 2011).

The IMB 2011C designed by the U.S. Cold Regions Research and Engineering Laboratory (CRREL) was deployed adjacent to ITP #47 (Figure 1). The data collected by the IMBs includes: ice drift, meteorological observations, ice mass balance, and atmosphere-ocean–ice temperature profiles. The IMB measures the elevations of the snow (or ice) surface and the ice base using acoustic sounders; vertical temperature profile from 1.0 m above the initial snow surface to 1–2 m below the initial ice bottom using a thermistor string with an interval of 0.1 m; and near-surface air temperature and pressure (Richter-Menge et al., 2006). The mass-balance information provides year-round high-resolution measurements of the accumulation and melt of snow and the growth and melt of ice, mostly focusing on melt rate at the top and bottom surfaces of the ice (Richter-Menge et al., 2006).

2.2 Site 2

The POPS instrument was deployed at 89.31°N, 142.11°W on April 12 in 2011, approximately 70 km away from Site 1, by the Japan Agency for Marine Earth Science and Technology (JAMSTEC) Arctic research team as a part of the North Pole Environmental Observatory Program (Figure 1). The POPS consists of an Argo-type subsurface CTD profiler and an ice platform (Kikuchi et al., 2007; Kawaguchi et al., 2012). The POPS profiler acquired temperature, conductivity and pressure in a depth range of 7 – 570 m with an interval of 1-2 m in depth, where the temperature and conductivity are recorded with a SBE 41CP CTD sensor from Sea-Bird Electronics with an accuracy of 0.01 PSU and 0.001 °C, respectively. It is tethered to a surface-unit that was mounted on a multi-year ice of ~1.9 m thickness. Sensors equipped with the surface-unit measures air temperature and pressure at 1 m height. The POPS collected oceanographic data when the underwater profiler ascends from the greatest depth, and the oceanographic sampling is performed one-way each day. The Iridium antenna was damaged, which caused sporadic data transmission. On day 191, a pressure ridge formed in webcam view of the POPS buoy which was not damaged. The POPS transmitted until day 239 (Vivier et al., 2016).

The Ice T buoys and POPS buoys were placed together with web cameras installed by the Polar Science Center (Applied Physics Laboratory, Seattle) (Vivier et al., 2016). The Ice T buoy records the parameters associated with the regional sea ice mass balance. Ice T included a 2-meter-long floating surface buoy and a subsurface instrument module that hangs 6 meters below

the ice base, called the "fish" here. The fish contains a Seabird SBE37 conductivity temperature sensor that records temperature and salinity nominally at 6 m below the ice/ocean interface. The sensor was calibrated with a temperature of 0.0002°C and a conductivity of 0.002 mS/cm (Vivier et al., 2016). The surface buoy with the vertical chain of 32 thermistors across the snow/ice/water layer measures temperatures. The air temperature, atmospheric pressure, GPS position, and the tilt of the instrument are also recorded (Vivier et al., 2016).

2.5 Data processing

Using observational data obtained by an Ice-Tethered Profiler and a POPS buoy, we compared the properties of the upper ocean water and the surface mixed layer depth between two locations. The mixed layer depth is estimated as the minimum depth in the first 100 m, where stability is maximum, determined as a maxima in $N^2$, where N is the Brunt-Vaisala frequency. The autonomous buoys drift with the perennial ice pack. Ice velocity time series were derived from the hourly GPS position fixes reported by the ITP and POPS buoys. Time series of mixed layer properties recorded with the ITP and POPS instruments are shown in figures 3 and 4. To estimate the heat content of the IOBL available for melting ice, the heat content relative to the in-situ freezing point was calculated for the surface layer at a depth of 7 m. For each CTD profile, freezing point of sea water was calculated as a function of salinity and pressure. This value was then used to calculate the departure from freezing at the depth of 7m following Shaw et al. (2009). The difference between in-situ temperature and in-situ freezing point are thermodynamically relevant at the ocean-ice interface, and indicate the melting or formation of ice (Stanton et al. 2012). Positive values indicate that the in-situ temperature is warmer than the freezing point and will cause melting. We applied a low-pass filter with a cutoff period of approximately 20 days to calculate a time series of ice drift velocity.

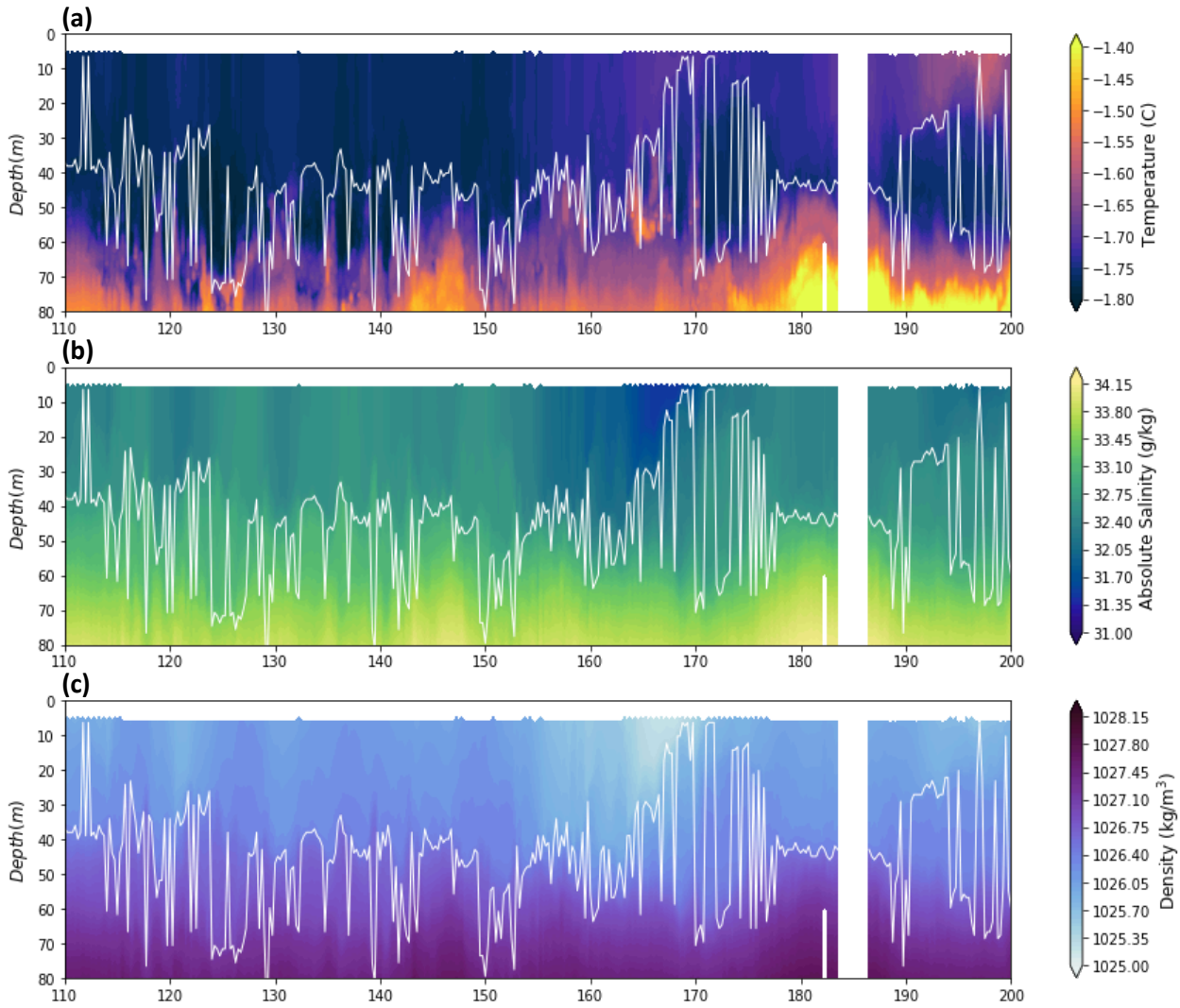


Figure 3. Time-depth contour plots of ITP #47;(a) temperature in °C, (b) absolute salinity in g/kg, and (c) density in kg/m$^3$. White segments indicate missing data. The white line indicates the mixed layer depth.

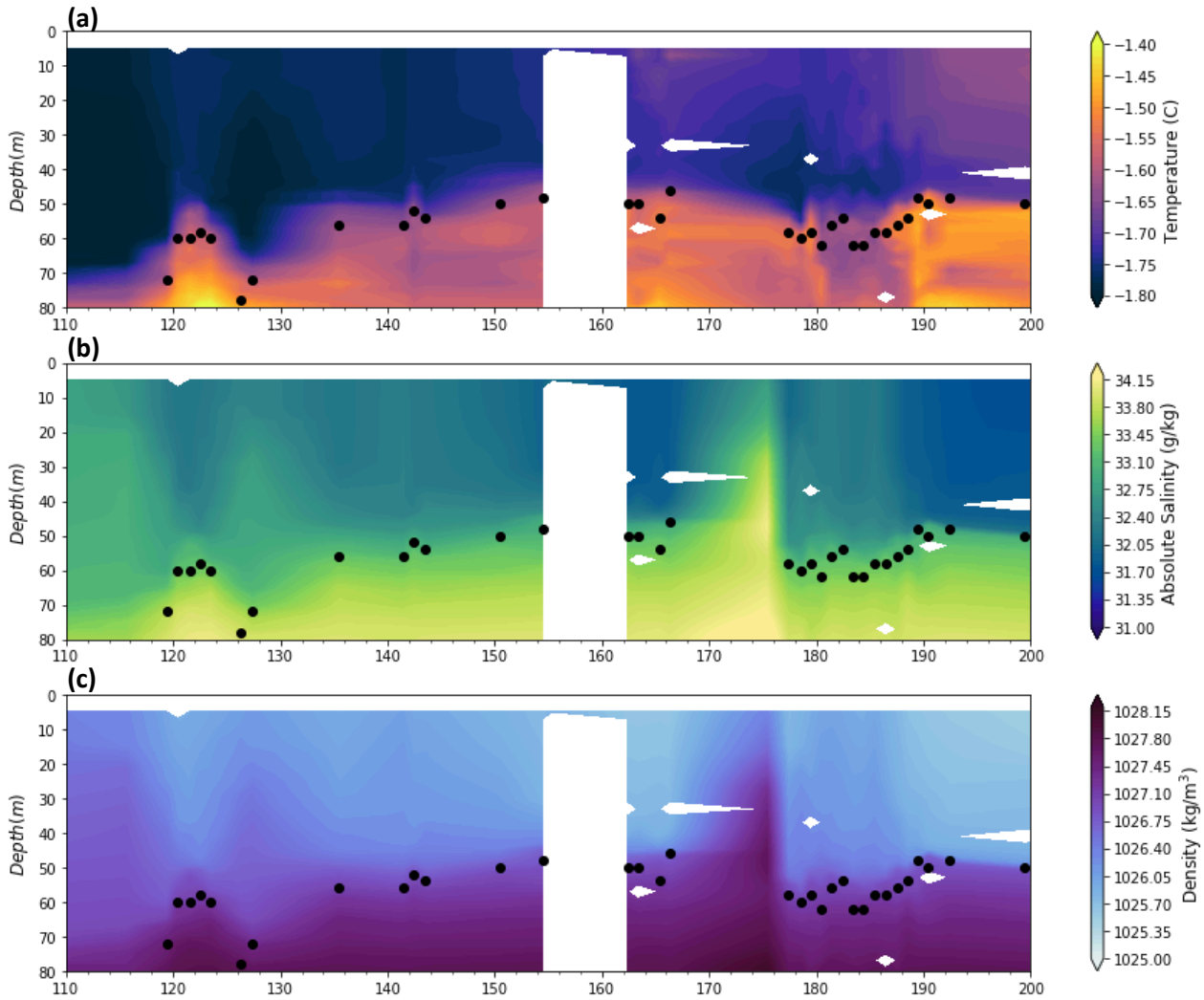


Figure 4. Identical to figure 3 for the POPS buoy in 2011. The black dots indicate the mixed layer depth.

## 3. Results

Comparing these two cases which were only about 70km apart indicates spatial variability associated with heat fluxes near the ice base. The two cases clearly show distinct spatial variations in the upper ocean properties and the mixed layer depth during the spring-summer transition, as well as the basal ice melt.

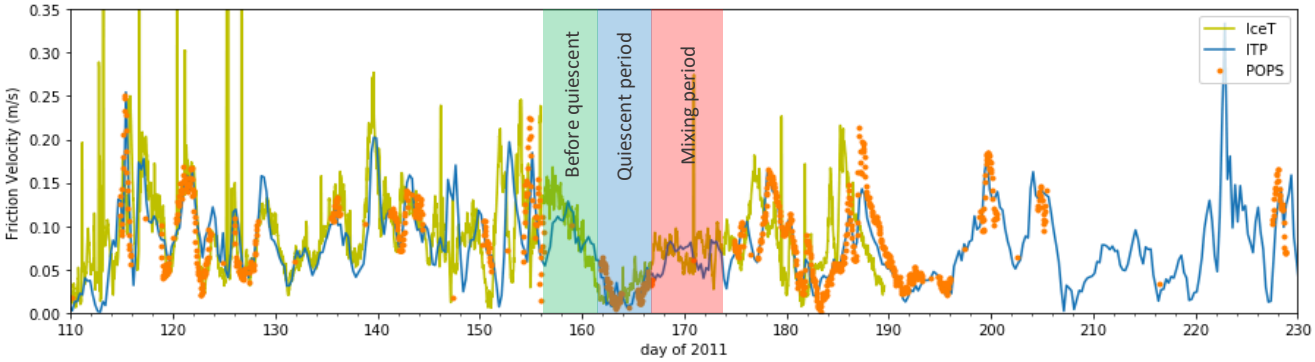


Figure 5. Ice velocity time series; ITP (blue), POPS (orange), and IceT (yellow); green shade indicates before quiescent period, blue shade indicates quiescent period, and red shade indicates mixing period.

*Friction velocity*

According to Hayes (2003) and Cole et al. (2014), the friction velocity is a key parameter controlling momentum flux, as it represents the overturning speed of energy-containing eddies. Figure 5 shows the time series of ice drift speed, which is correlated to friction velocity (Cole et al., 2017). The speed pattern shown in Figure 5 is nearly identical between the two sites. In Site 1, near motionless periods (speed of 0-0.05 m/s) occurred during days 162-166, days 192-196, and days 207-209. In Site 2, the motionless periods occurred during days 162-166, days 182-184, and days 190-196. Figure 6 shows the velocity of sea ice and surface temperature below the ice for Site 1 and Site 2, respectively. During the quiescent periods, at both sites the 7m temperature below the ice correspondingly increases (Figure 6), which indicates surface layer warming during the quiescent periods. At low drift speeds, mixing of the surface layer is low. Incoming solar radiation warms the top 10m and is not mixed deeper. Therefore, warm layer can be formed that freshens if ice is melted.

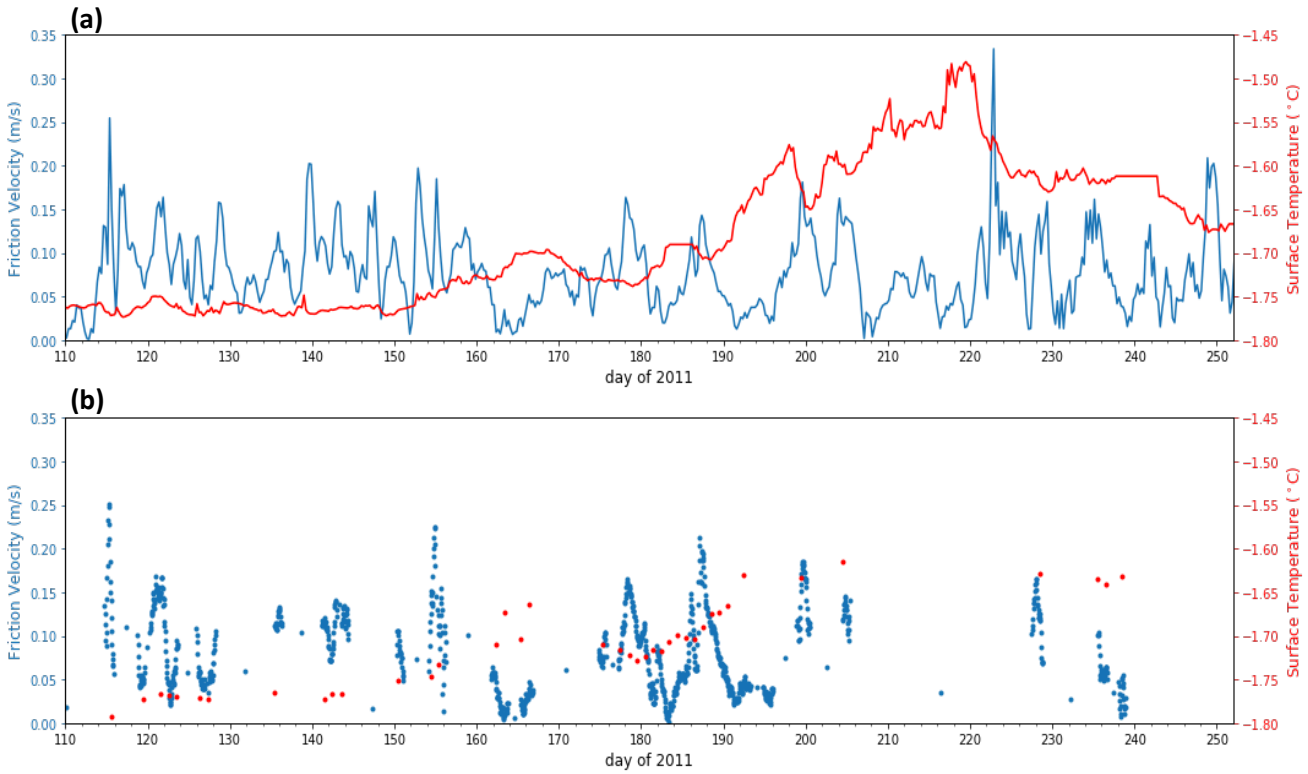


Figure 6. The drift velocity of the sea ice and surface temperature; **(a)** indicates Case 1 and **(b)** indicates Case 2.

At Site 1, shown in Figure 3b, freshening occurred during days 163-168, and a distinctive meltwater lenses formed on the surface. After day 160 ice velocity decreases, a fresh layer formed and was mixed into deeper water after day 170 (Figure 3). This corresponds to the time when the departure from the freezing point started to increase above zero (Figure 7). During days 192-198, slight freshening also occurred near the surface, and surface warming occurred (Figure 3). After day 200 this warm water was mixed into the deeper layer.

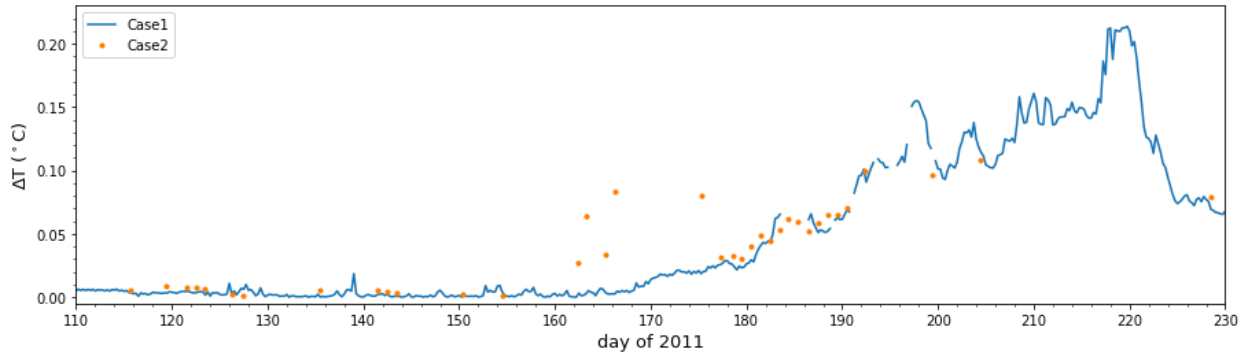


Figure 7. Time series of temperature departure from freezing point; Site 1 (blue) and Site 2 (orange)

Likewise, at Site 2, shown in Figure 4b, surface freshening occurred during days 162-166 and days 190-196 with meltwater lenses formed and surface layer warming, then, as the velocity increased after the quiescent periods, the warm layer was mixed into the deeper layer. Low ice motion decreases kinetic mixing and enhances heating from solar radiation near the ocean surface, and melt results in development of a shallow stratification. This shallow fresh warm layer promoted upward heat flux to the ice and basal melt, but gets mixed deeper as soon as ice drift begins to increase (Vivier et al., 2016).

Since both sites experienced similar quiescent and mixing periods, and similar solar warming, we hypothesized that stratification controls the differences in basal melt. In order to observe changes in surface seawater through the different periods and compare the two sites, we consider a case study for one of the quiescence periods. We regard days 162-166 as the quiescent period, days 158-162 as before quiescent periods and days 167-172 as mixing periods. We refer to this case study as Case 1 and Case 2 for Sites 1 and 2, respectively.

*Comparison of water properties in Case1 and Case 2*

Changes of water properties in the upper ocean layer influence the heat flux to the sea ice base. Ice melt or growth influence the mixed layer water properties and depth. The mixed layer influences ice by warming the ice if the temperature goes above freezing or when changes in the stability of the water influence the transfer of momentum to the ice. In figures 3 and 4, depth-time contour plots from ITP and POPS buoys show the upper ocean properties and indicate the mixed layer depth. Between days 118 and 123, while Case 1 showed fluctuations in mixed layer depth, ranging between 26-71m, a slight shoaling of the surface mixed layer occurred in Case 2 with mixed layer depth decreasing from 72m to 58m. During days 118 and 123, the slight difference in friction velocity, shown in Figure 5, could lead to the difference in changes of mixed layer depth. On day 120, while Case 1 is at speed of 0.07m/s, Case 2 is at speed of 0.03m/s (Figure 5).

Low ice speed is associated with warming and freshening within a very shallow surface layer (Vivier et al., 2016). Both Case 1 and Case 2 experienced a continuous surface freshening from day 162 to day 166, decreasing surface salinity from 32.7 to 31.5 and from 32.1 to 31.8, respectively. Near days 162 and 166, continuous surface warming within the mixed layer was observed in both Case 1 and Case 2, increasing surface temperature from -1.74 °C to -1.70 °C

and from -1.74 °C to -1.66 °C, respectively (Figure 6). This suggests increased solar input. Between days 192 and 200, surface warming within the mixed layer was observed in both Case 1 and Case 2. However, surface freshening within the mixed layer was more clearly observed in Case 2 than Case 1. The freshening of surface water in Site 2 happens about 20 days earlier than Site 1 occurring from day 180.

Departure from the freezing temperature is used to estimate the heat content of the IOBL that is available for melt. We suggest solar input to the upper ocean could be a driver of melt onset in Site 2. Departure from the freezing temperature, shown in Figure 7, shows temperature above freezing point occurred between days 162-174, at 7m depth, in Case 2, but not in Case 1. Due to poor time resolution in POPS data, we do not know the ocean state between days 128 and 135, days 154 and 162, days 166 and 174, days 193 and 198, and days 205 and 238.

Nonetheless, two observations suggest a driver of the earlier melt onset of Case 2. Our result agrees with the finding of Vivier et al. (2016) that during these days the Ice-T sensor recorded the highest water temperature at 6m below the ice for the entire observation period. The significant temperature deviations from the freezing point suggest an input of heat by solar radiation while leads in the vicinity of Site 2 remained open and unfrozen (Vivier et al., 2016).

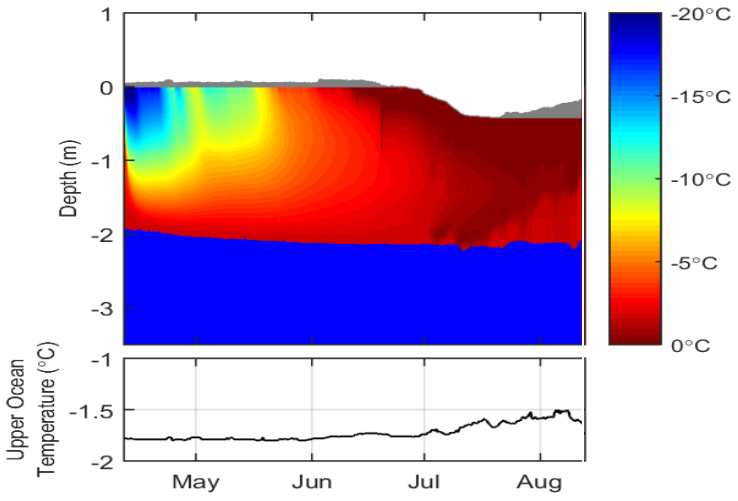


Figure 8. Sea ice temperature data from Ice Mass Balance (IMB) buoy program (Case1). Figure reproduced from Perovich et al. (2011).

*Basal melt*

An IMB buoy that was deployed adjacent to ITP #47 (Case 1) showed ice thickness decreased by approximately 40 cm between days 175 and 190 during late summer. The onset of basal ice melting was observed in mid-July (Figure 8). In contrast, in Case 2, the onset of basal melt occurred in mid-May; the basal ice melt gradually increased with time until day 165. Basal ice melting is related to solar warming and mixing driven by transition from low to high ice motion. Quiescent periods can cause warmer waters beneath the cooler fresher waters of the sea ice, which potentially leads to basal melt onset. After the quiescent period, upwelling from warm water below the pycnocline occurred due to the increased vertical mixing.

We compared the different water masses in the upper 50m of Case 1 and Case 2 before quiescence, during quiescent and subsequent mixing periods in order to observe variability between the two cases in the entrainment of warmer waters. This may shed light on the different basal melt onset timing. We have isolated two occurrences of surface freshening followed by mixing that happened concurrently at Site 1 and Site 2. We consider one of these periods in this thesis. Days 162-166 are considered as the quiescent period when the buoy array is virtually motionless at speed of 0-0.05m/s, and the following days 167-175 are considered as mixing periods. Days 158-162 are referred to as before quiescent period.

In Case 1, in Figures 9 and 10, transition from before quiescent to quiescent period was time coincident with surface layer freshening with a decrease of 3g/kg in salinity (figure 9b & 10b) and surface layer warming with increased temperature about 0.02 °C (figure 9a & 10a) at depth 6m. At depths between 44 and 60m, the temperature profiles are distinctively different, with Site 1 having the warmest layer during the quiescent period. This may suggest a localized warm water intrusion in this layer. Since it is not likely to warm at 44m depth by the increasing solar during the case study, the localized warm water intrusion could be either a remnant warm layer from previous summer or lateral intrusion. During the transition from quiescent to mixing periods, the warm and saline water layer at depth of 46-60m was entrained up to the surface layer because of the weak and unstable density gradient (figure 10c).

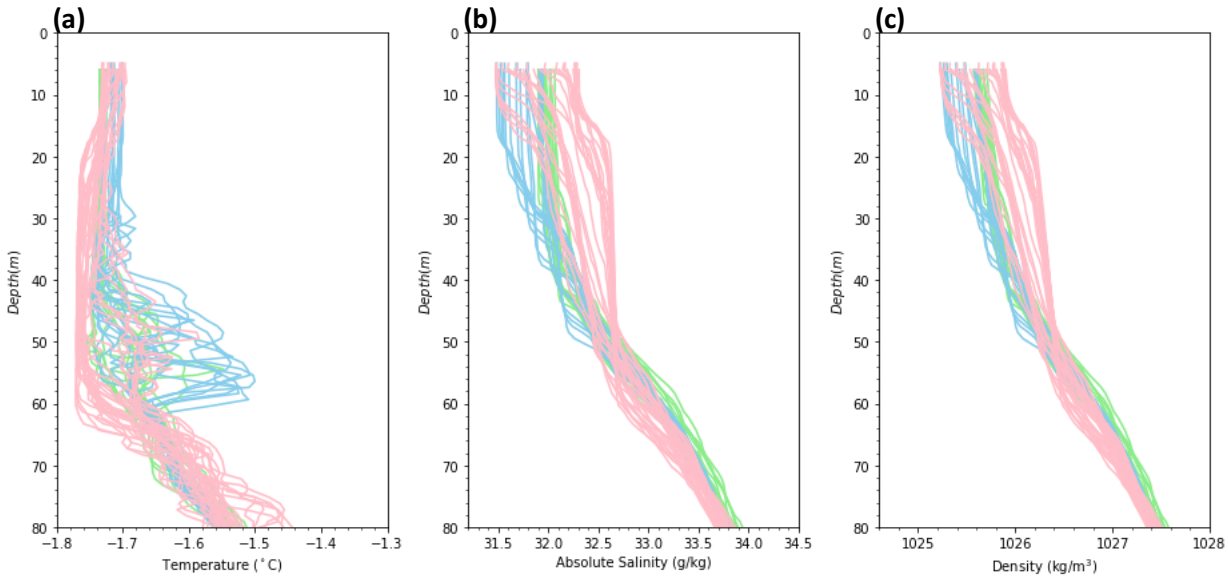


Figure 9. The **Case 1** vertical profiles during before quiescent period (doy158-162, light green), during quiescent period (doy162-166, sky-blue) and mixing period (doy167-175, pink); (a) temperature in °C, (b) absolute salinity in g/kg, and (c) density in kg/m$^3$

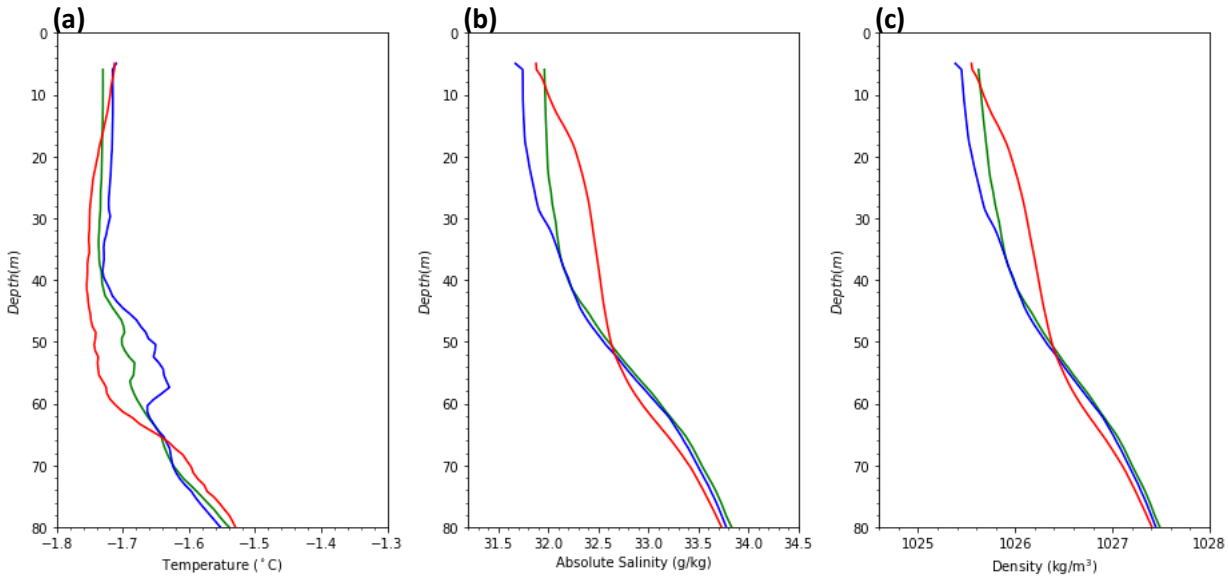


Figure 10. The averaged vertical profiles of **Case 1** during before quiescent period (doy158-162, green), during quiescent period (doy162-166, blue) and mixing period (doy167-175, red); (a) temperature in °C, (b) absolute salinity in g/kg, and (c) density in kg/m$^3$

On the other hand, in Case 2, the vertical profiles before quiescent and during quiescent periods are nearly identical (Figure 11 & 12). During the transition from quiescent to mixing periods, it is apparent that water below the halocline was entrained to the surface (figure 11a & 12b) and the density gradient became unstable and weaker (figure 11c & 12c). However, in figure 10a, the pycnocline deepens about 6m from depth at 42m to 48m, and the surface layer at 6m becomes cooler by about 0.04 °C.

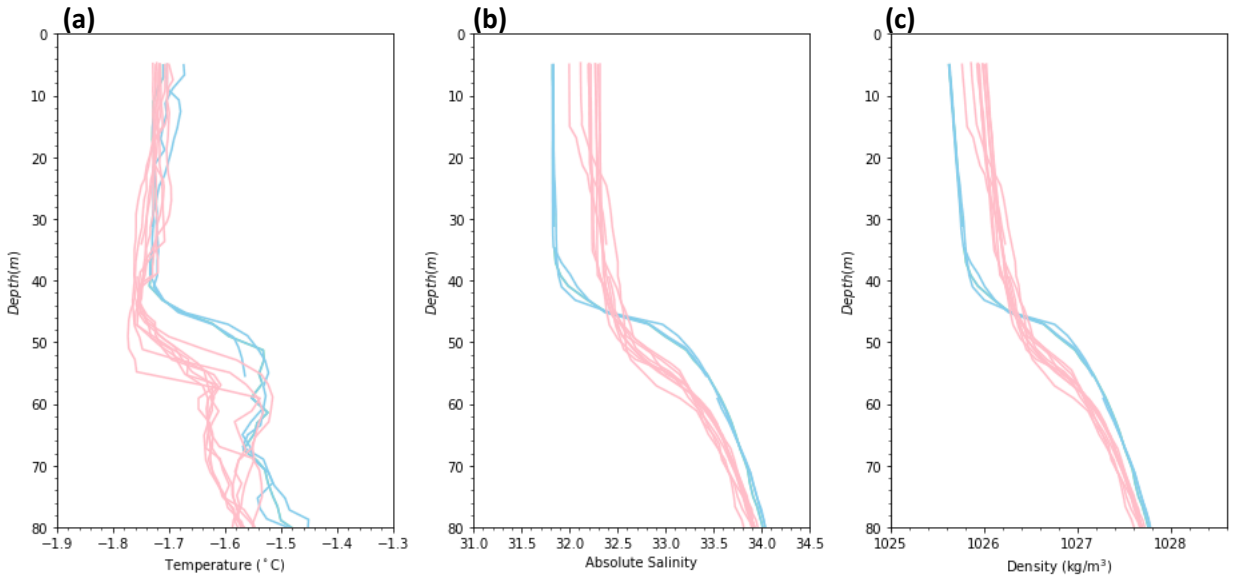


Figure 11. The **Case 2** vertical profiles during before quiescent period (doy158-162, light green), quiescent period (doy162-166, sky-blue) and mixing period (doy167-175, pink); (a) temperature in °C, (b) absolute salinity in g/kg, and (c) density in kg/m$^3$

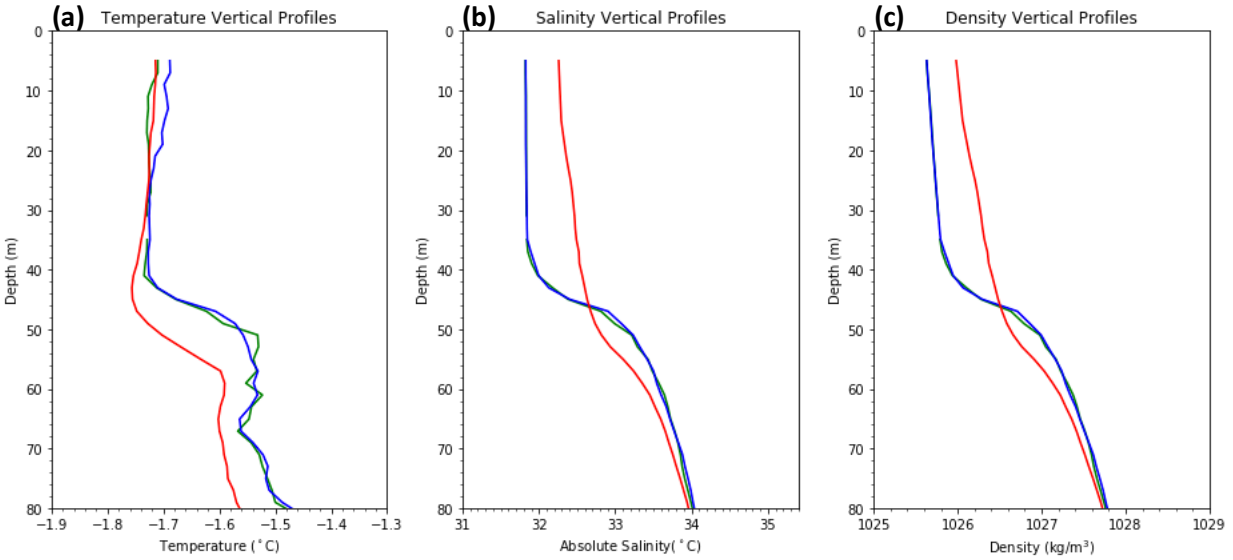


Figure 12. The averaged vertical profiles of **Case 2** during before quiescent period (doy158-162, green), during quiescent period (doy162-166, blue) and mixing period (doy167-175, red); (a) temperature in °C, (b) absolute salinity in g/kg, and (c) density in kg/m$^3$

The vertical profiles of water properties from Case 1 and Case 2 during the before quiescent, quiescent and mixing periods, shown in Figures 13, 14 and 15, respectively, clearly show the distinctive spatial difference of the change in water mass when it transits from

quiescent to mixing periods. During the quiescent period, days 162-166, Case 2 is more stratified than Case 1, showing greater temperature, salinity and density gradients from depth at 42m to 50m (Figure 14). In Figure 15, during the mixing period, days 167-175, the surface layer of Case 2 is slightly warmer and more saline, with stronger stratification than Case 1. Increased ice motion during mixing periods enhanced kinetic mixing, which can promote upward heat flux to the ice which may be associated with basal melt in Case 2. Comparing changes in stratification during the transition, Case 2 has changed more significantly than Case 1 with large changes in density gradient (figure 13c, 14c & 15c). This might suggest a greater change in stratification of Case 2 lead to more turbulent mixing and more entrainment of warm water from below the surface layer, thereby potentially causing earlier basal melt onset. In Vivier et al., (2016), in Case 2 the thin summer surface layer begins to thicken through entrainment of melt water.

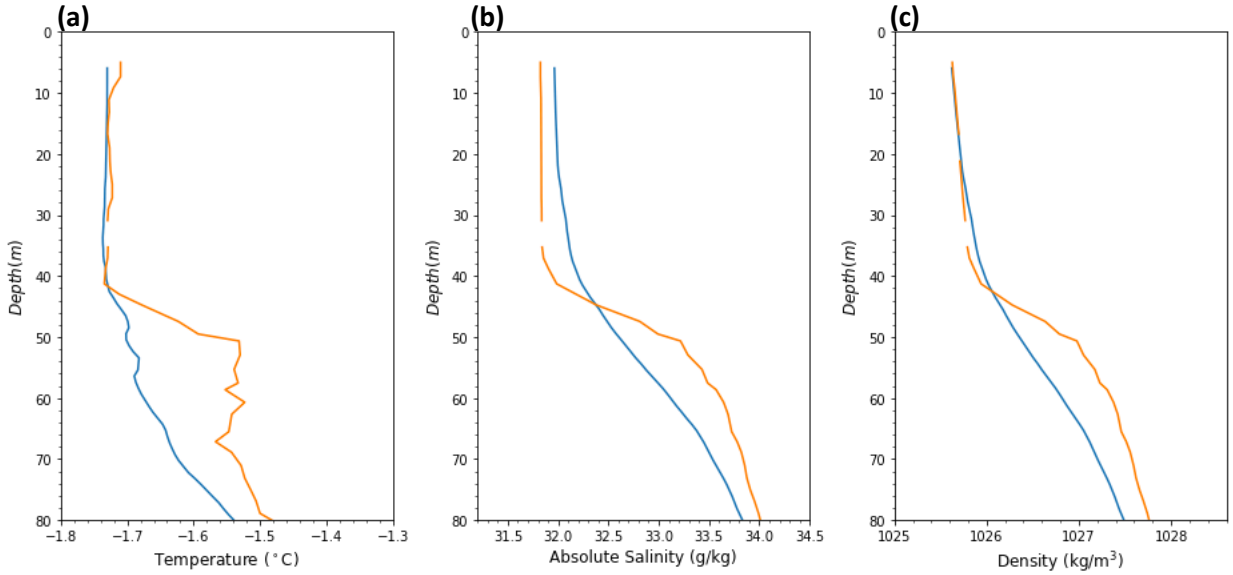


Figure 13. The averaged vertical profiles of **Case 1** (ITP, blue) and **Case 2** (POPS, orange) before quiescent conditions, doy162-166; (a) temperature in °C, (b) absolute salinity in g/kg, and (c) density in kg/m$^3$.

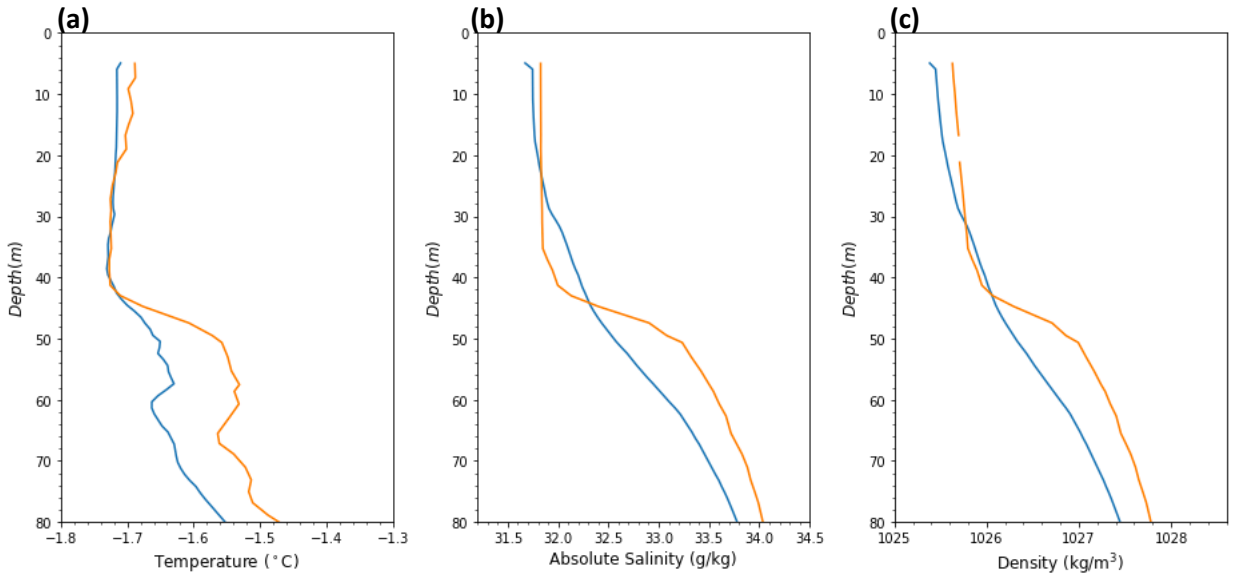


Figure 14. The averaged vertical profiles of **Case 1** (ITP, blue) and **Case 2** (POPS, orange) during quiescent conditions, doy162-166; (a) temperature in °C, (b) absolute salinity in g/kg, and (c) density in kg/m$^3$.

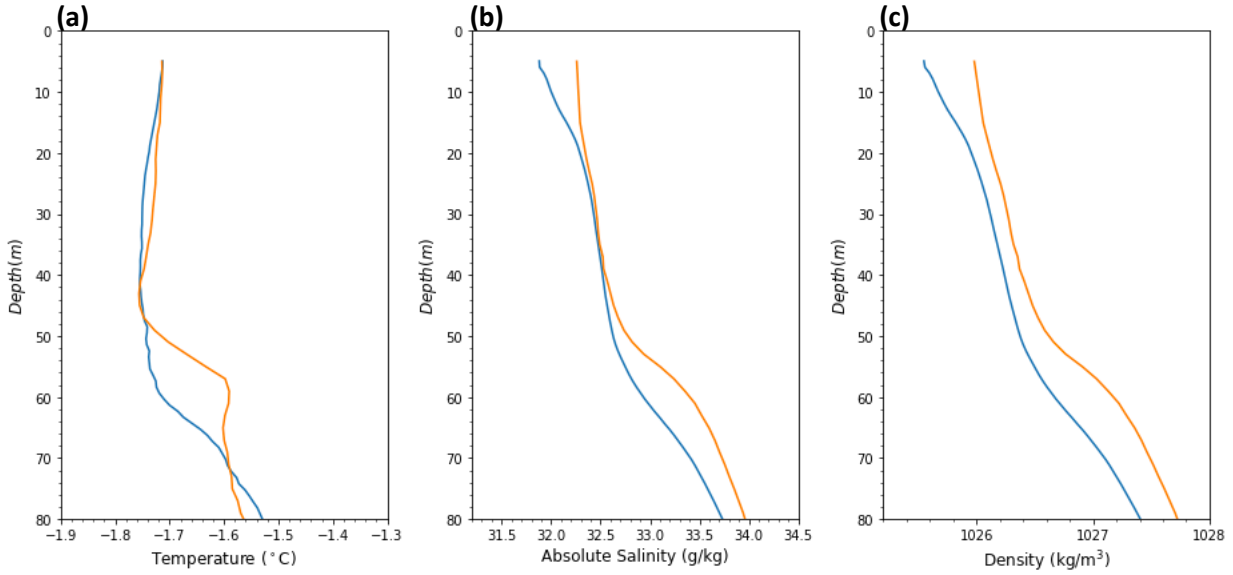


Figure 15. The averaged vertical profiles of **Case 1** (ITP, blue) and **Case 2** (POPS, orange) during mixing conditions, doy167-175; (a) temperature in °C, (b) absolute salinity in g/kg, and (c) density in kg/m$^3$.

A T-S diagram (Figure 16) shows the T-S properties of the upper 100m water for the two cases. While the surface layer of Case 1 became fresher by about 0.02 g/kg during the transition from quiescent to mixing periods with nearly constant temperature, that of Case 2 became

fresher about by about 0.2 g/kg and slightly warmer. Although the dilution effect can be seen along the path in both cases as the condition changes from the quiescent condition to the mixing condition, the pattern of change in Arctic surface water and subsurface layer are different between Case 1 and Case 2. While in Case 1, surface water became cooler and the subsurface layer became warmer, in Case 2, both surface water and subsurface layer became cooler and saltier.

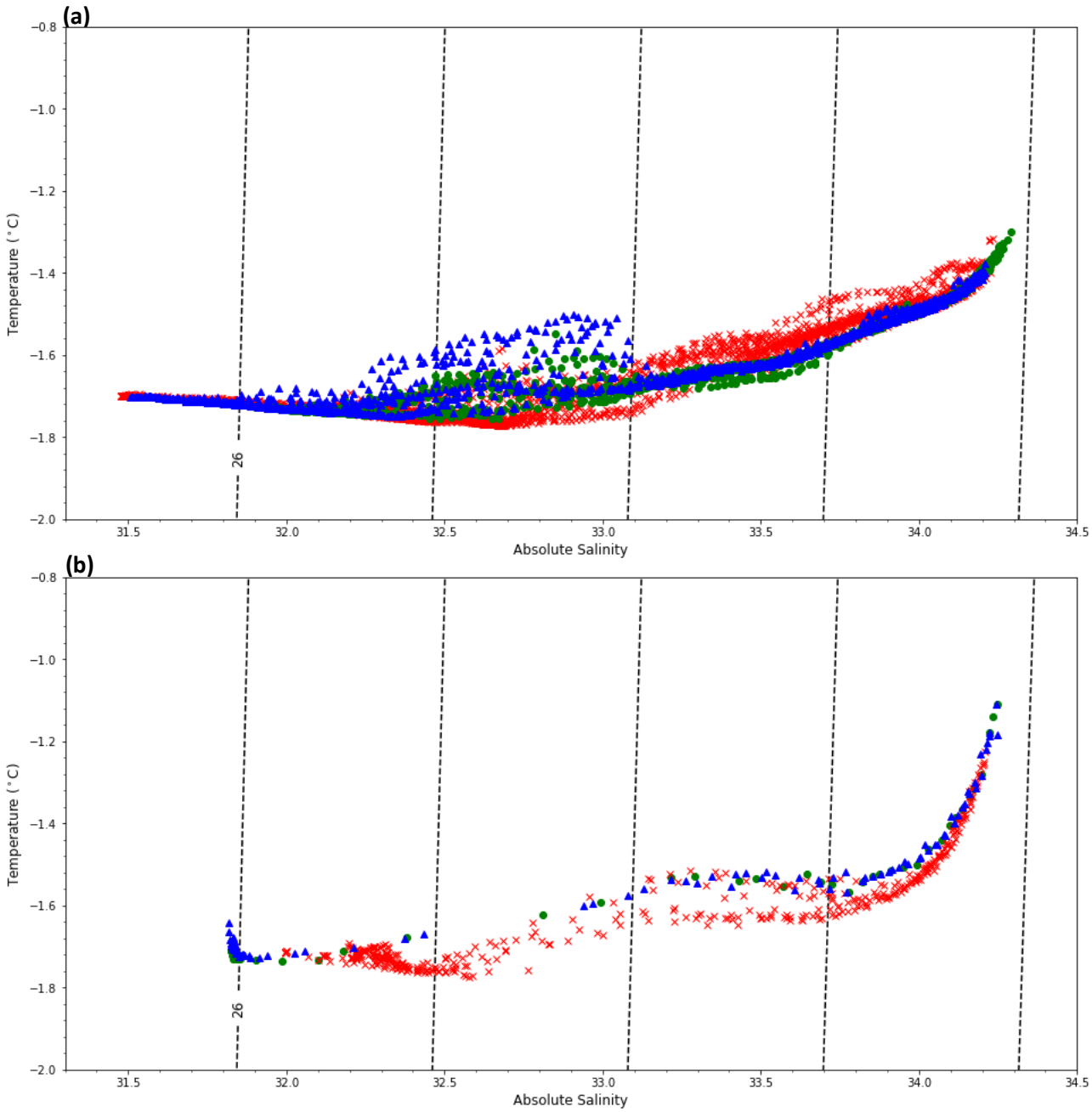


Figure 16. T-S diagram of the upper 100m ocean; green circles indicate before quiescent period; blue triangles indicate during quiescent period; red crosses indicated mixing period. (a) indicates Case 1 and (b) indicates Case 2.

## 4. Summary and Discussion

A primary objective of this study is to investigate how spatial variability within the surface mixed layer, associated with variability in heat fluxes to the ice base by comparing two cases approximately 70km of each other. We found considerable difference in surface water properties, ice basal melt onset and wind-driven mixing between Case 1 and Case 2. The transfer of solar energy into the upper ocean are comparable between the two cases.

Considering heat budget in the IOBL, heat flux from ocean to sea ice is variable (McPhee et al., 2005). It is related to the heat content in the IOBL, turbulence in the IOBL, and the stratification of the pycnocline below the IOBL (Shaw et al., 2009). While surface melt is affected by clouds, incident solar radiation, start and end dates of melting period, air temperature and wind, basal melt is related to heat content of the IOBL, ice-ocean mixing, solar input to the upper ocean and ice concentrations (Perovich & Richter-Menge, 2015). Using SHEBA observations, Stanton et al. (2012) observed that enhanced solar radiation input into IOBL results in larger ocean-to-ice heat fluxes and ice melt. Solar radiation absorbed in leads plays a major role in basal melt; as the area of open water increases, solar radiation input to IOBL increases, thereby ultimately increasing basal melt (Perovich & Richter-Menge, 2015).

The departure from the freezing point is closely related to basal melt or growth of sea ice. We observed that the melt onset of Site 2 occurred about 20 days earlier than that of Site 1. Early melt onset allows an earlier expansion of open water between the ice floes, which increases solar absorption that warms the IOBL. Heat stored from solar radiation in the IOBL can enhance the heat flux from the upper ocean to sea ice (Stanton et al., 2012). The heat flux in the IOBL is controlled by increasing heat storage marked by the departure from freezing point (Shaw et al., 2009). The departure from freezing point is a measure of how far the in-situ temperature of a layer is from the freezing point of sea water, which represents the heat available for basal melt (Shaw et al., 2009). In figure 6, we identified that Case 2 departs from the freezing point much earlier and becoming larger than Case 1 during the day 162-176. However, the observations for Case 2 during this period are sparse in space and time, which prevents confident conclusion. Nonetheless, the enhanced heat would promote basal melt.

If the two sites are assumed to have approximately the same amount of solar radiation input during the period days 110 - 200, earlier melt onset at Site 2 indicates the enhanced

stratification and reduced downward mixing enhances heat flux to the ice. One potential mechanism to enhance basal melt is entraining warmer water from below the mixed layer by wind-driven ice motion. Sea ice motion is mainly driven by atmospheric forcing (Thorndike & Colony, 1985). Under the mixing condition in which ice speeds are high, the mixed layer remains well-mixed and becomes more saline, with a potential to deepen the mixed layer under strong surface stress (Hayes, 2003). On the other hand, under quiescent conditions, low ice motion results in a reduced turbulent mixing, which allows heat from solar radiation to accumulate in the IOBL (Vivier et al., 2016). This causes the development of the freshening surface layer with a shallow stratification (Vivier et al., 2016). During the quiescent period, fresh water does not mix vertically because of the strong and stable density gradient near the surface and low ice speeds. During the quiescent period at Site 2, with the stronger stratification in the upper ocean due to sea ice melt, heat content is stored in the upper pycnocline is suspected to be increasing as the surface water becomes warming and freshening. The transition between the quiescent and ice drift periods sees increase in kinetic mixing that can change stratification. During the mixing period, as the stratification at Site 2 becomes eroded, the weaker stratification might cause increased vertical mixing and entrainment of warm water into the surface with higher heat content, possibility causing earlier basal melt onset. Basal melt of sea ice or reduction in the growth rate can occur due to the entrainment of these warmer waters beneath the cooler fresher waters of the mixed layer. Oceanic forcing affects sea ice and causes basal melt by turbulent mixing (Perovich et al., 2002; Shaw et al., 2009).

Considering the warm layer underneath at Site 1, shown in Figure 9a, the heat contained in this layer could come from solar heat collected in the previous summer or the later heat flux from regional eddies. We do not know the source of the warm layer. However, considering the vertical energy budget, we can track where the heat that is entrained to the mixed layer comes from. Looking at the temperature vertical profiles, shown in Figure 14a, the heat content for depths near the surface above 10m is smaller than that of depths below 40m during the quiescent period in both cases. The heat and salt flux due to solar and melt is smaller compared to the upward mixing after the quiescent period. The heat budget of the surface layer is related to solar heat and latent heat. Since the solar heat is used up to melt the sea ice, the little bump is shown below the surface water, freshening the water (Figure 14). Thus, the water below contains more heat available to be entrained to the mixed layer than the water above. Looking at the T-S

diagram (Figure 16), we can identify how the warm water masses mix vertically for this particular event. At Site 1, during the mixing period, the water below moves up and the water above moves down (Figure 16a). The heat from the water below will move upward into the surface mixed layer, which is more than the heat coming from the sunlight. On the other hand, at Site 2, Figure 16b does not show the warmer water below mixes upward, which suggests more solar energy accumulates in the shallower layer. However, due to lack of information on what fluxes actually entrain into the mixed layer, it is not possible to directly determine what effect the accumulated heat over time had on earlier basal melt onset at Site 2.

When the two cases experienced the transition from quiescent to mixing conditions, Case 1 began to cross to the Lomonosov Ridge while Case 2 stayed on the Eurasian basin near Lomonosov Ridge (Figure 2). Across the Lomonosov Ridge, abrupt and large changes in water mass properties occurs (Anderson et al., 1994; Rudels et al., 1997). The change across the Lomonosov Ridge was pronounced throughout the intermediate layer. The intermediated water below the Atlantic layer was warmer and more saline in the Makarov Basin than in the Eurasian Basin (Rudels et al., 1994). The different basal melt onset of the two cases may be related to differing upper ocean stability in the two basins, and the differing characteristics of water mass properties between them. The shift of Case 1 from the Makarov Basin to the Lomonosov Ridge might cause changes in stability and stratification due to the shift of water mass properties on the different basins. In contrast, Case 2 does not experience the shift of the water mass properties. However, Site 2 shows a transition in water properties.

There are several ways for heat to enter the Arctic upper ocean: through sensible and radiative fluxes into the upper ocean through thin ice, open water, and leads through, Pacific water, Atlantic Water, and summer input of warm river water (Carmack et al., 2015). While heat input as sensible heating and river inputs are immediately available to the ice through direct contact with floe edges and advection under floes, heat input by Atlantic Water and Pacific Water is separated from the surface by stratification (Carmack et al., 2015). Through double diffusion, a process that drives heat and salt fluxes due to the difference in their molecular diffusivities, heat and salt of warm Atlantic Water and Pacific Water can move up to the surface mixed layer (Carmack et al., 2015). Also, shear related to internal wave and boundary layer may drive the vertical fluxes of heat and salt (Carmack et al., 2015). Several questions triggered by our case study could be investigated in future work; how much of the heat entrained into the

surface mixed layer is from the heating from the warm water mass below. Vivier et al. (2016) identified there were lead openings nearby at Site 2 with the large opening in mid-June. Open leads and thin ice can promote heating near the surface and heat accumulated in the surface layer, melt enhances a shallow stratification, promoting ice melt. We know that the heat and salt flux due to solar input and sea ice melt is smaller compared to the upward mixing after the quiescent period. For the future studies of basal met, we need to consider the localized water stability conditions as well as the ocean dynamics, and quantify how much heat from water above moves downward and how much heat from water below moves upward.

We observed that these two cases have significant spatial difference in upper water properties and melt onsets during spring-summer transition. During surface layer freshening, variability in lead opening and ice motion controls the spatial variability in the mixed layer as well as the basal melt associated with heat flux from the upper ocean to the bottom of the sea ice. The different water mass characteristics vary by basin, resulting from differing vertical heat transport caused by differences in stratification and vertical mixing. The data from autonomous buoys are crucial to improve our understanding of the basal ice melt onset. To improve the understanding of relations between the spatial variability and the energy budget of water mass properties under sea ice, our results suggest we need a quantitative analysis of the processes driving the onset of basal ice melt, as well as more accurate dataset at several sites across the oceanic mesoscale. It is important to resolve variability in the ocean below the pycnocline as well as have several time series resolving variability in the upper ocean and basal melt.

**Acknowledgments**

First and foremost, I'd like to thank my thesis advisor Jennifer K. Hutchings for your exceptional support for a year. You gave me the opportunity to pursue undergraduate research and senior thesis. You have always been generous with your advice. You have provided valuable feedback and always guide me through both this thesis and my course of studies and gave me so many suggestions, hints, and feedback. Thanks to you, I was able to learn Python and you provided me with a lot of resources to help me improve Python skills. This has become a great asset to me. It's been a real pleasure to pursue the thesis of relevant research in the Arctic. I am also grateful for the help and advice Emily Shroyer has given me, especially for sharing great ideas and in-depth knowledge in interpreting energy budget in the upper ocean. I would also like to thank Yusuke Kawaguchi for sharing his POPS data that helped contribute to my research. The ITPs measurements are transferred to servers at the Woods Hole Oceanographic Institution (Krishfield et al., 2008; Toole et al., 2011). The ITP data used are available at www.whoi.edu/itp.

## References


Aagaard, K., Swift, J., & Carmack, E. (1985). Thermohaline circulation in the Arctic Mediterranean seas. Journal of Geophysical Research. C. Oceans, 90(C3), 4833–4846. Retrieved from http://search.proquest.com/docview/14196054/

Anderson, L. G., G. Bjork, O. Holby, E. P. Jones, G. Kattner, K. P. Koltermann, B. Liljeblad, R. Lindegren, B. Rudels, and J. Swift. (1994). Water masses and circulation in the Eurasian Basin: Results from the Oden 91 expedition, J. Geophys. Res., 99, 3273–3283.

Arndt, S., & Nicolaus, M. (2014). Seasonal cycle and long-term trend of solar energy fluxes through Arctic sea ice. The Cryosphere, 8(6), 2219–2233. https://doi.org/10.5194/tc-8-2219-2014

Björk, G., Jakobsson, M., Assmann, K., Andersson, L. G., Nilsson, J., Stranne, C., & Mayer, L. (2018). Bathymetry and oceanic flow structure at two deep passages crossing the Lomonosov Ridge. Ocean Science, 14(1), 1–13. https://doi.org/10.5194/os-14-1-2018

Carmack, Polyakov, Padman, Fer, Hunke, Hutchings, … Winsor. (2015). Toward quantifying the increasing role of oceanic heat in sea ice loss in the new Arctic. Bulletin of the American Meteorological Society, 96(12), 2079–2105. https://doi.org/10.1175/BAMS-D-13-00177.1

Cole, S., Timmermans, M.-L., Toole, J., Krishfield, R., & Thwaites, F. (2014). Ekman Veering, Internal Waves, and Turbulence Observed under Arctic Sea Ice. Journal of Physical Oceanography, 44(5), 1306–1328. https://doi.org/10.1175/JPO-D-12-0191.1

Cole, S. T., Toole, J. M., Lele, R., Timmermans, M.-L., Gallaher, S. G., Stanton, T. P., & Shaw, W. J. (2017). Ice and ocean velocity in the Arctic marginal ice zone: Ice roughness and momentum transfer. Elementa: Science of the Anthropocene, 5(17). https://doi.org/10.1525/elementa.241

Comiso, J. C., Parkinson, C. L., Gersten, R., & Stock, L. (2008). Accelerated decline in the Arctic sea ice cover. Geophysical Research Letters, 35(1), n/a–n/a. https://doi.org/10.1029/2007GL031972

Curry, J., Schramm, J., Ebert, E., & Curry, JA. (1995). Sea ice-albedo climate feedback mechanism. Journal of Climate, 8(2), 240–247. https://doi.org/10.1175/1520-0442(1995)0082.0.CO;2

Hayes, D., & Washington Univ Seattle Applied Physics Lab. (2003). The Heat and Salt Balances of the Upper Ocean Beneath a Spatially Variable Melting Sea Ice Cover. Retrieved from http://www.dtic.mil/docs/citations/ADA422484

John M. Toole, Richard A. Krishfield, Mary-Louise Timmermans, & Andrey Proshutinsky. (2011). The Ice-Tethered Profiler: Argo of the Arctic. Oceanography, 24(3), 126–135. https://doi.org/10.5670/oceanog.2011.64

Kawaguchi, Hutchings, Kikuchi, Morison, & Krishfield. (2012). Anomalous sea-ice reduction in the Eurasian Basin of the Arctic Ocean during summer 2010. Polar Science, 6(1), 39–53. https://doi.org/10.1016/j.polar.2011.11.003

Kikuchi, Inoue, & Langevin. (2007). Argo-type profiling float observations under the Arctic multiyear ice. Deep-Sea Research Part I, 54(9), 1675–1686. https://doi.org/10.1016/j.dsr.2007.05.011

Krishfield, R., Toole, J., Proshutinsky, A., & Timmermans, M.-L. (2008). Automated Ice-Tethered Profilers for Seawater Observations under Pack Ice in All Seasons. Journal of Atmospheric and Oceanic Technology, 25(11), 2091–2105. https://doi.org/10.1175/2008JTECHO587.1

Markus, T., Stroeve, J. C., & Miller, J. (2009). Recent changes in Arctic sea ice melt onset, freezeup, and melt season length. Journal of Geophysical Research: Oceans, 114(C12), n/a–n/a. https://doi.org/10.1029/2009JC005436

McPhee, M., Kwok, R., Robins, R., and Coon, M. (2005). Upwelling of Arctic pycnocline associated with shear motion of sea ice. Geophys. Res. Lett. 32:L10616. doi: 10.1029/2004GL021819

Thorndike, A. S., and R. Colony, Sea ice motion in response to geostrophic winds, J. Geophys. Res., 87(C8), 5845-5852, 1982.

Perovich, D. K., Grenfell, T. C., Light, B., and Hobbs, P. V. (2002). Seasonal evolution of the albedo of multiyear Arctic sea ice, Journal of Geophysical Research: Oceans, 107. doi:10.1029/2000JC000438

Perovich, D. K. (2007). Light reflection and transmission by a temperate snow cover, Journal of Glaciology, 53, 201–210. doi:10.3189/172756507782202919

Perovich, D.K., J. Richter-Menge, and C. Polashenski. (2011). Observing and understanding climate change: Monitoring the mass balance, motion, and thickness of Arctic sea ice, http://imb-crrel-dartmouth.org.

Perovich, D. K. & Polashenski, C. (2012). Albedo evolution of seasonal Arctic sea ice, Geophysical Research Letters, 39. doi:10.1029/2012GL051432

Perovich, D. K., & Richter-Menge, J. A. (2015). Regional variability in sea ice melt in a changing Arctic. Philosophical Transactions. Series A, Mathematical, Physical, and Engineering Sciences, 373 (2045). https://doi.org/10.1098/rsta.2014.0165

Richter-Menge, J. A., Perovich, D. K., Elder, B. C., Claffey, K., Rigor, I., & Ortmeyer, M. (2006). Ice mass-balance buoys: a tool for measuring and attributing changes in the thickness of the Arctic sea-ice cover. Annals of Glaciology, 44, 205–210. https://doi.org/10.3189/172756406781811727

Rudels, B., E. P. Jones, L. G. Anderson, and G. Kattner (1994), On the intermediate depth waters of the Arctic Ocean, in The Polar Oceans and Their Role in Shaping the Global Environment, Geophys. Monogr. Ser., vol. 85, edited by O. M. Johannessen, R. D. Muench, and J. E. Overland, pp. 33–46, AGU, Washington, D. C.

Schauer, U., B. Rudels, E. P. Jones, L. G. Anderson, R. D. Muench, G. Björk, J. H. Swift, V. Ivanov, and A.-M. Larsson. (2002). Confluence and redistribution of Atlantic water in the Nansen, Amundsen and Makarov basins, Ann. Geophys., 20(2), 257–273.

Shaw, W. J., T. P. Stanton, M. G. McPhee, J. H. Morison, and D. G. Martinson (2009), Role of the upper ocean in the energy budget of Arctic sea ice during SHEBA, J. Geophys. Res., 114, C06012, doi:10.1029/2008JC004991.

Stanton, T. P., Shaw, W. J., & Hutchings, J. K. (2012). Observational study of relationships between incoming radiation, open water fraction, and ocean-to-ice heat flux in the Transpolar Drift: 2002–2010. Journal of Geophysical Research: Oceans, 117(C7), n/a-n/a. https://doi.org/10.1029/2011JC007871

Stroeve, J., Holland, M. M., Meier, W., Scambos, T., & Serreze, M. (2007). Arctic sea ice decline: Faster than forecast. Geophysical Research Letters, 34(9), n/a–n/a. https://doi.org/10.1029/2007GL029703

Toole, J. M., R. A. Krishfield, M.-L. Timmermans, and A. Proshutinsky. (2011). The ice-tethered profiler: Argo of the Arctic, Oceanography, 24(3), 126–135, doi:10.5670/oceanog.2011.64.

Swift, J., Jones, E., Aagaard, K., Carmack, E., Hingston, M., Macdonald, R., … Perkin, R. (1997). Waters of the Makarov and Canada basins. Deep-Sea Research Part II, 44(8), 1503–1529. https://doi.org/10.1016/S0967-0645(97)00055-6

Vivier, Frédéric, Jennifer K. Hutchings, Yusuke Kawaguchi, Takashi Kikuchi, James H. Morison, Antonio Lourenço, and Tomohide Noguchi. (2016). Sea Ice Melt Onset Associated with Lead Opening during the Spring/summer Transition near the North Pole. Journal of Geophysical Research: Oceans 121.4 (2016): 2499-522.

Woodgate, R. A., Aagaard, K., Muench, R. D., Gunn, J., Björk, G., Rudels, B., … Schauer, U. (2001). The Arctic Ocean Boundary Current along the Eurasian slope and the adjacent Lomonosov Ridge: Water mass properties, transports and transformations from moored instruments. Deep-Sea Research Part I, 48(8), 1757–1792. https://doi.org/10.1016/S0967-0637(00)00091-1